MOLECULAR AND CELLULAR BIOLOGY, Feb. 2003, p. 1239–1250 Vol. 23, No. 4
0270-7306/03/$08.00+0 DOI: 10.1128/MCB.23.4.1239–1250.2003

Human Nudel and NudE as Regulators of Cytoplasmic Dynein in Poleward Protein Transport along the Mitotic Spindle

Xiumin Yan, Fang Li, Yun Liang, Yidong Shen, Xiangshan Zhao, Qiongping Huang, and Xueliang Zhu*

Laboratory of Molecular Cell Biology, Institute of Biochemistry and Cell Biology, Shanghai Institutes for Biological Sciences, Chinese Academy of Sciences, Shanghai 200031, China

Received 7 October 2002/Returned for modification 16 November 2002/Accepted 25 November 2002

Emerging evidence supports the idea that a signaling pathway containing orthologs of at least mammalian NudE and Nudel, Lis1, and cytoplasmic dynein is conserved for eukaryotic nuclear migration. In mammals, this pathway has profound impact on neuronal migration during development of the central nervous system. Lis1 and dynein are also involved in other cellular functions, such as mitosis. Here we show that Nudel also participates in a subset of dynein function in M phase. Nudel was specifically phosphorylated in M phase in its serine/threonine phosphorylation motifs, probably by Cdc2 and also Erk1 and -2. A fraction of Nudel bound to centrosomes strongly in interphase and localized to mitotic spindles in early M phase. By using mutants incapable of or simulating phosphorylation, we confirmed that phosphorylation of Nudel regulated the cell-cycle-dependent distribution, possibly by increasing its dissociation rate at the microtubule-organizing center. Moreover, phosphorylated Nudel or the phosphorylation-mimicking mutant bound Lis1 more efficiently. We further demonstrated that a Nudel mutant incapable of binding to Lis1 impaired the poleward movement of dynein and hence the dynein-mediated transport of kinetochore proteins to spindle poles along microtubules, a process contributing to inactivation of the spindle checkpoint in mitosis. These results point to the importance of Nudel-Lis1 interaction for the dynein activity in M phase and to a possible role of Nudel phosphorylation as facilitating such interaction. In addition, comparative studies suggest that NudE is also functionally related to its paralog, Nudel.

In *Aspergillus nidulans*, nuclear distribution genes (*Nud*s) are those important for even distribution of nuclei along hypha. Among them, *NudA*, *NudG*, and *NudI* encode the heavy, light, and intermediate chains, respectively, of the cytoplasmic dynein complex (2, 34, 35), which is a microtubule minus-end-directed motor essential for microtubule-based cell motility (15). *NudF* interacts with *NudA* genetically and is essential for the function of dynein (33). *NudE* is identified as a multicopy suppressor of *NudF* and may therefore code for an effector of NudF protein (6).

The *Nud* pathway is also conserved in mammals. Mammalian cytoplasmic dynein is a large protein complex composed of two heavy chains (DHC) of ~550 kDa, three to four 74-kDa intermediate chains (DIC), four light-intermediate chains of 55 kDa, and light chains of 8 to 22 kDa (5, 11, 16). As a motor, it is involved in multiple cellular activities, such as organelle organization and intracellular transport (5, 11, 16). It is also critical for centrosome and spindle assembly by recruiting proteins like pericentrin, γ-tubulin, and NuMA (5, 17, 36). Recently, dynein was found to contribute to inactivation of the spindle checkpoint, a mechanism that guarantees equal separation of chromatids into daughter cells, by transporting spindle checkpoint proteins from kinetochores to the spindle poles along spindle microtubules (13, 14).

The mammalian homologue of NudF is Lis1. Its haploinsufficiency causes type I lissencephaly, a brain disease characteristic of smooth brain due to deficient neuronal cell migration during development of the central nervous system (CNS) (12, 23, 24). Lis1 interacts with DHC and DIC (25, 28, 31). It positively regulates the retrograde movement of dynein, mitotic spindle orientation, and mitotic progression through interaction with dynein (8, 28, 31).

There are two highly related NudE homologues in mammals, NudE and NudE-like (Nudel). Both proteins directly interact with Lis1 and dynein (9, 20, 25). NudE and Nudel interact with Lis1 through their N-terminal coiled-coil domains (9, 25). When overexpressed in *Xenopus*, the coiled-coil domain of murine NudE serves as a dominant-negative mutant and blocks CNS lamination (9). In addition, human Nudel interacts with DHC of dynein, while murine NudE binds to the light chain (9, 20, 25). Nevertheless, whether Nudel and NedE have roles in mitosis is presently not known.

Emerging evidence suggests that phosphorylation of Nudel and NudE plays important roles in neuronal migration. Nudel contains five proline-dependent serine/threonine phosphorylation (S/TP) motifs. It is highly expressed in the brain and is phosphorylated at the first three S/TP motifs by Cdk5/p35, a brain-specific kinase critical for axon outgrowth, axon guidance, and neuronal migration in the developing cerebral cortex (3, 4, 20, 25, 27). Cdk5 colocalizes with Nudel in the cell bodies and growth cones of embryonic hippocampal neurons (20). Inhibition of phosphorylation by using either a Nudel mutant or the Cdk5 inhibitor roscovitine induces neuritic swelling (20). Together with the involvement of NudE in CNS lamination, Nudel and NudE appear to link the Cdk5 signaling pathway to the Lis1/dynein pathway. In addition, localization of Nudel and

* Corresponding author. Mailing address: Institute of Biochemistry and Cell Biology, 320 Yue Yang Rd., Shanghai 200031, China. Phone: 86-21-64315030, ext. 2156. Fax: 86-21-64338357. E-mail: xlzhu@sibs.ac.cn.

NudE at centrosomes also implies that they have a role in the cell cycle (9, 20, 25).

All the S/TP motifs of Nudel are conserved in murine NudE and MP43, a *Xenopus* homologue, while the latter two proteins also contain an additional S/TP motif resembling a typical Cdc2 site (SPNR) at their C termini (9, 20, 25, 30). MP43 is specifically phosphorylated by mitotic extracts from *Xenopus* eggs in vitro, suggestive of a phosphoprotein in M phase (30).

In this study, we explored properties of Nudel and NudE in mitosis. We found that both proteins were subjected to M-phase-dependent reorganization correlated with phosphorylation. Our results also indicated involvement of both proteins in cytoplasmic dynein-mediated transport of mitotic checkpoint proteins from kinetochores to spindle poles in M phase.

MATERIALS AND METHODS

Plasmid constructs. To express FLAG-tagged proteins, cDNAs were properly inserted into pUHD30F, a vector derived from pUHD20 (41). The cDNA for full-length human Nudel was obtained from a yeast two-hybrid clone, pACT2-Nudel, which encoded an extra 33 amino acids upstream of the first methionine. The cDNA for NudE was amplified from a human placenta cDNA library (Clontech) by PCR and confirmed by sequencing with the reference sequence under GenBank accession no. AK000108. FLAG-Nudel^{mt5} contained S198A, T219V, S231A, S242A, and T245V mutations in the S/TP motifs created by PCR mutagenesis. In contrast, FLAG-Nudel^{pmt5} contained S198E, T219E, S231E, S242E, and T245E mutations to simulate phosphorylation. Mutants Nudel^{S1} to Nudel^{S5} was made from the sequence coding for FLAG-Nudel^{mt5} so that each mutant contained only one distinct S/TP motif.

Green fluorescent protein (GFP)-tagged NudE, Nudel, and mutants were expressed from plasmids constructed in pEGFP-C1 (Clontech). To express maltose-binding protein (MBP) fusion protein in *Escherichia coli* for antibody production, the 2.1-kb *Eco*RI-*Bgl*II fragment from pACT2-Nudel was cloned into pMAL-CR1 (New England Biolabs). The immunogen contained residues 39 to 345 of Nudel. Bub1 cDNA was amplified by PCR and was subcloned into pUHD30F.

Antibody production. After affinity purification with amylose resin (New England Biolabs), the MBP-Nudel fusion protein was used to immunize chicken. Immunoglobulin Y (IgY) was purified from egg yolks by polyethylene glycol (PEG) precipitation (10). After incubation of total IgY with excess amounts of MBP immobilized on amylose resin, specific antibodies to Nudel were affinity-purified by using the immunogen immobilized on Hybond-C membrane (Amersham), as described previously (26).

Cell culture and cell cycle synchronization. All cell lines were maintained in Dulbecco's modified Eagle's medium (DMEM; GIBCO) supplemented with 10% (vol/vol) calf serum (Sijiqing Company, Hangzhou, China) in an atmosphere containing 5% CO_2. Cell cycle synchronization with hydroxyurea and nocodazole (Sigma) was described previously (40).

ATP inhibitor assay. The ATP inhibitor assay was performed as described previously (13, 14). Briefly, after transfection with appropriate plasmids for 36 h, HEK293T cells were rinsed twice with phosphate-buffered saline to remove culture medium and were soaked in saline plus 5 mM Na-azide and 1 mM 2-deoxyglucose (DOG; Fluka) at 37°C. To disassemble microtubules, cells were cultured in the presence of 2 μg of nocodazole/ml for 3 h prior to ATP inhibitor assay in the presence of nocodazole. Images were collected live at 37°C or after fixation by using a cold CCD SPOT II (Diagnostic) on an Olympus BX51 microscope.

Preparation of mitotic cell extracts. SMMC-7721 cells were blocked in mitosis as described previously (40). Mitotic cells (10^8) were shaken off and harvested. The mitotic extracts were prepared as described previously (21). Briefly, the mitotic cell pellet was resuspended in 0.5 ml of extraction buffer (50 mM Tris-HCl [pH 7.4], 250 mM NaCl, 1 mM EDTA, 50 mM NaF, 1 mM dithiothreitol, 0.1% Triton X-100, and protease inhibitors). The cells were lysed by brief sonication and then were centrifuged at 12,000 rpm in a Sorvall Biofuge Fresco for 20 min at 4°C. The supernatant was collected and stored at −70°C in aliquots.

Immunoprecipitation and kinase assay. After transfection for 36 h, HEK293T cells were collected. FLAG-tagged Nudel or mutants from ~10^7 cells were immunoprecipitated with anti-FLAG M2 beads (Sigma) and were eluted with 0.8 mg of FLAG peptide/ml in a total volume of 30 μl (39).

The kinase assays were performed in a 40-μl reaction volume containing 8 μl of eluted FLAG-tagged proteins, 4 μl of 10× kinase buffer, 50 μM ATP, 5 μCi of [γ-^{32}P]ATP, and 0.5 μl of the mitogen-activated protein kinase (MAPK) Erk2 (100 U/μl; New England Biolabs) or Cdc2 (20 U/μl; New England Biolabs). The mixtures were incubated for 30 min at 30°C. The reactions were stopped with 2× sodium dodecyl sulfate (SDS) sample buffer. For the reaction mixtures containing mitotic cell extracts, transfected cells were lysed with radioimmunoprecipitation assay buffer and were immunoprecipitated with anti-FLAG beads (Sigma). The reaction mixture, containing 2.5 μl of 10× kinase buffer, 50 μM ATP, 5 μCi of [γ-^{32}P]ATP, and 5 μl of mitotic cell extracts, was preincubated at 30°C for 10 min in the presence of 50 μM olomoucine (Promega) or equal volumes of the solvent dimethyl sulfoxide (DMSO). The anti-FLAG beads containing the immunocomplex were added to the mixture, which was incubated for an additional 20 min. The beads were then washed twice with 1 ml of radioimmunoprecipitation assay buffer and were suspended in 30 μl of 2× SDS sample buffer.

Isolation of centrosomes. Centrosomes were isolated from ~6×10^7 HEK293T cells transiently expressing GFP-tagged Nudel, Nudel^{mt5}, or Nudel^{pmt5} as described previously (18). Briefly, after nocodazole treatment for 1 h the cells were harvested and resuspended in 2 ml of cold 0.1× Tris-buffered saline–8% (mass/vol) sucrose buffer. A solution of 4 ml of lysis buffer (1 mM HEPES [pH 7.2], 0.5% NP-40, 0.5 mM $MgCl_2$, 0.1% β-mercaptoethanol, and protease inhibitors) was added. Cells were then disrupted with 5 strokes in a glass homogenizer. The homogenate was immediately centrifuged at 2,500 × *g* for 10 min. Sixty microliters of 1 M HEPES (pH 7.2) and 6 μl of (1 mg/ml) DNase I were added to the supernatant and were incubated for 30 min on ice. The lysate was then placed on top of 3.5 ml of 60% sucrose solution and was spun at 10,000 × *g* for 30 min. The 60% sucrose fraction containing centrosomes was recovered and diluted to 20 to 25% with distilled water. This suspension was added to the top of a discontinuous sucrose gradient (from the bottom to the top, containing 1.7, 1, and 1 ml of 70, 50, and 40% sucrose solutions, respectively) in a 13-ml SW28 Beckman ultraclear tube. Following centrifugation at 40,000 × *g* for 1 h, 18 fractions (170 μl each) were collected, starting from the bottom of the gradient. The fractions were stored at −80°C after being frozen in liquid nitrogen.

Western blotting and immunofluorescence microscopy. Immunoblotting and indirect immunofluorescence (IIF) microscopy were performed with appropriate antibodies as described previously (40, 41). For IIF, cells were fixed in cold methanol for 20 min. To remove soluble proteins, CV1 cells were extracted for 1 min with an extraction buffer (20 mM Tris-Cl [pH 7.0], 100 mM NaCl, 300 mM sucrose, 3 mM $MgCl_2$, 1 mM EGTA, 0.5% Triton X-100) before fixation. Rabbit anti-GFP antibody and goat anti-Lis1 antibody were from the Santa Cruz Biotechnology Company. The rest of the primary antibodies were from Sigma. Alkaline phosphatase-conjugated and peroxidase-conjugated secondary antibodies were purchased from Promega; rhodamine-conjugated goat anti-mouse IgG and IgM were purchased from Pierce, Inc. Fluorescein isothiocyanate-conjugated secondary antibodies were from the Sino-American Biotechnology Company (Shanghai, China). Immunoblots probed with peroxidase-linked secondary antibodies were visualized by enhanced chemiluminescence (Amersham), while those that used phosphatase-linked antibodies were developed by using 5-bromo-4-chloro-3-indolylphosphate/nitroblue tetrazolium substrates (Promega). IIF images were digitized by using a cold CCD SPOT II (Diagnostic) on an Olympus BX51 microscope. For time-lapse microscopy, the same exposure time was used for each cell. In addition, fluorescence shutters were opened only during exposure to avoid bleaching. Quantitation of IIF images as gross brightness (0 to 256/pixel) was performed as described previously (13) by using Adobe Photoshop software. The fluorescence intensity of each centrosome was measured by subtracting background intensity from total intensity in selected centrosomal areas. Illustrations for publication were organized by using Adobe Photoshop software and were exported from an EPSON Stylus Photo 890 printer.

Nucleotide sequence accession number. The sequence data for the cDNA of Nudel (initially named Mitap1) have been submitted to the GenBank database under accession number AF182078.

RESULTS

Antibody production. We identified Nudel as a protein associated with the kinetochore protein mitosin in a yeast two-hybrid screen by using the kinetochore-binding regions of mitosin as bait (data not shown) (40, 42). To study its biological functions, we generated specific polyclonal antibodies in chickens by using an MBP fusion containing residues 39 to 345 of Nudel as immunogen. Specific IgY was purified by affinity

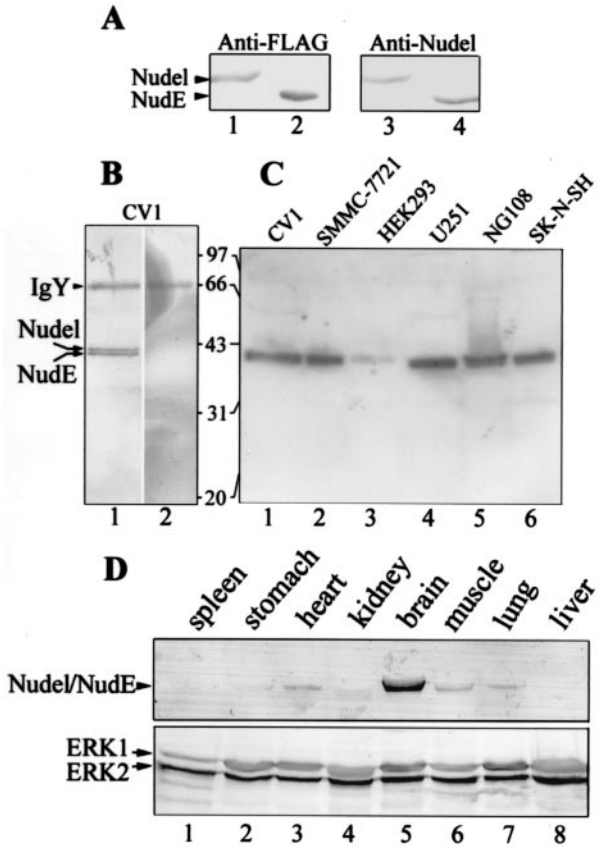

FIG. 1. Biochemical properties of cellular Nudel and NudE. (A) Specificity of anti-Nudel IgY. HEK293T cells expressing either FLAG-Nudel (lanes 1 and 3) or FLAG-NudE (lanes 2 and 4) were lysed and subjected to SDS–10%PAGE and immunoblotting with the indicated antibodies. Endogenous Nudel and NudE were not detected in lanes 3 and 4 due to their low expression levels. (B) Identification of cellular Nudel and NudE in CV1 cells. Anti-Nudel IgY preincubated with 10 μg of either MBP (lane 1) or MBP-Nudel (lane 2) was used for immunoblotting. (C) Detection of Nudel and NudE in a variety of cell lines with anti-Nudel IgY. Fifteen micrograms of total proteins was used for each indicated cell line. (D) Distribution of Nudel and NudE in mouse tissues. Twenty micrograms of total proteins was used for each indicated tissue. Immunoblotting was performed with anti-Nudel IgY (upper panel) or anti-ERK1 and anti-ERK2 antibodies to show equal loading (lower panel).

chromatography (10, 26). Purified IgY specifically recognized bacterial Nudel but not MBP (data not shown). Nudel and NudE are highly related proteins in mammals, with an identity of ~53%. As shown in Fig. 1A, the IgY antibody actually recognized both FLAG-Nudel (lane 3) and FLAG-NudE (lane 4).

To identify cellular Nudel and NudE, CV1 lysate was immunoprecipitated and then immunoblotted by using purified IgY. A doublet of ~40 kDa was detected (data not shown). To confirm that the doublet was related to Nudel, two aliquots of IgY were incubated with 10 μg of MBP or the immunogen, respectively. As shown in Fig. 1B, preincubation with MBP did not affect recognition of the doublet (lane 1); in contrast, treatment with the immunogen completely blocked the antibody, as expected (lane 2). Since human Nudel is just 10 residues longer than NudE, the doublet appeared to correspond to both proteins.

Purified IgY recognized protein bands of ~40 kDa in a variety of cell lines, including CV1, human hepatoma SMMC-7721, human embryonic kidney HEK293, human astrocytoma U251, mouse neuroblastoma and rat glioma hybrid cell line NG108-15, and human neuroblastoma SK-N-SH (Fig. 1C). Nudel and NudE were therefore widely distributed, with relatively low levels in HEK293 (Fig. 1C, lane 3). Further studies with mouse tissues indicated that the proteins were highly expressed in brain tissue (Fig. 1D, lane 5), which was in agreement with other reports (20, 25). Nudel and NudE were also expressed in heart (Fig. 1D, lane 3), skeletal muscle (lane 6), and lung (lane 7) tissue. In contrast, they were almost undetectable in spleen (Fig. 1D, lane 1), stomach (lane 2), kidney (lane 3), and liver (lane 8) tissue.

Phosphorylation of Nudel and NudE in M phase. To investigate the expression patterns of the Nudel family proteins during the cell cycle, SMMC-7721 cells were synchronized at G_1/S, S, M, and G_1 phase, respectively (40). The extent of synchrony was monitored by flow cytometry. The sample synchronized at the G_1/S boundary by using hydroxyurea was estimated to be 53.1% in G_1, 30.2% in S, and 16.7% in G_2/M. An S-phase sample was collected after release from the G_1/S boundary for 4 h; its cell cycle profile was 71.5% in S, 19.9% in G_1, and 8.6% in G_2/M. An M-phase sample was collected by mitotic shake-off after hydroxyurea and nocodazole blocking; its cell cycle distribution was 91.8% in G_2/M, 2.1% in G_1, and 6.1% in S. A G_1-phase sample was prepared by releasing a portion of the M-phase sample for 6 h; its cell cycle profile was 59.0% in G_1, 10.0% in S, and 30.0% in G_2/M. Microscopic examination of 4′,6′-diamidino-2-phenylindole (DAPI)-stained cells indicated that, in this G_1 sample, the mitotic index was less than 5%. Cells in this G_1 sample were indeed mainly in interphase.

Immunoblotting indicated a distinct pattern of Nudel and NudE in the cell cycle. In SMMC-7721 cells, only a single band was detected in interphase (Fig. 2A, lanes 1 to 3). The protein level in S phase was two- to threefold higher than those in G_1 and G_1/S. Detection of a doublet in CV1 but of only a single band in SMMC-7721 might suggest differential distribution of both proteins (9, 20, 25). In M phase, however, multiple bands appeared (Fig. 2A, lane 4). Their slower migration in SDS-polyacrylamide gel electrophoresis (PAGE) excluded the possibility of degradation but favored posttranslational modification. A homologue of Nudel in *Xenopus*, MP43, has been shown to be phosphorylated by mitotic extract in vitro but not by interphase extract (30). Since phosphorylation of MP43 also results in similar migration changes (30), we reasoned that the band shift of Nudel and NudE in M phase might also be due to phosphorylation.

To test if Nudel and NudE were indeed phosphorylated, the proteins were immunoprecipitated from SMMC-7721 cells synchronized in M phase and were treated with calf intestinal alkaline phosphatase (CIAP). After CIAP treatment the protein band migrated to the same position the interphase Nudel and NudE did (Fig. 2B, lanes 1 and 2). In contrast, the migration of mock-treated Nudel was not affected (Fig. 2B, lane 3). The slower migration bands were therefore phosphorylated forms of Nudel and NudE.

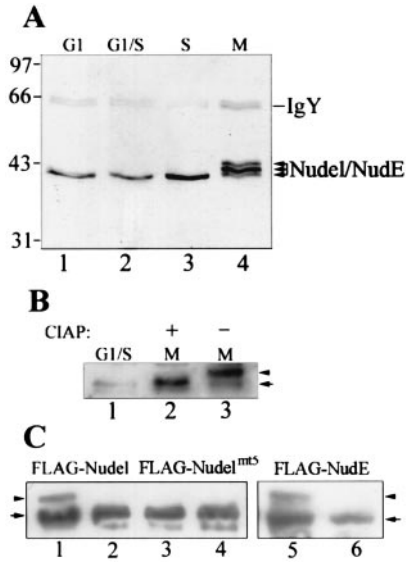

FIG. 2. Phosphorylation of Nudel and NudE in M phase. (A) Specific modification of Nudel and NudE in M phase. Human hepatoma SMMC-7721 cells were synchronized at the indicated stages of the cell cycle prior to lysis. Nudel and NudE were immunoprecipitated from 200 μg of total proteins and were detected by immunoblotting with anti-Nudel IgY. (B) CIAP assay. After immunoprecipitation from mitotic SMMC-7721 lysate, half of the beads were treated either with 10 U of CIAP (lane 2) or with just buffer (lane 3). The arrow and arrowhead point to the fast and slow migration forms, respectively. (C) Phosphorylation of both Nudel and NudE in M phase. After transfection of HEK293T cells for 24 h, half of the cells were treated with nocodazole for an additional 12 h (lanes 1, 3, and 5), while the rest (lanes 2, 4, and 6) were maintained as unsynchronized controls. Cell lysates were subjected to immunoblotting with anti-FLAG antibody.

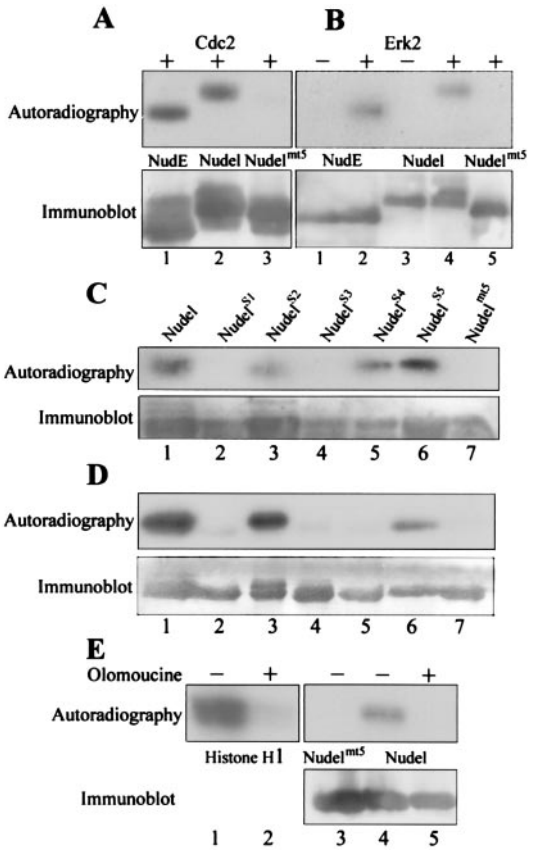

FIG. 3. Phosphorylation by Cdc2 and Erk2. (A) Phosphorylation by Cdc2 in vitro. FLAG-tagged NudE, Nudel, and Nudel^{mt5} were immunoprecipitated with anti-FLAG beads and were treated with purified Cdc2 in the presence of [γ-^{32}P]ATP. (B) Phosphorylation by Erk2 in vitro. Similar kinase assays were performed with or without purified Erk2 as indicated. (C) Phosphorylation sites in Nudel by Cdc2. FLAG-tagged Nudel^{S1} to Nudel^{S5}, each of which contained only one distinct S/TP motif, were immunoprecipitated and subjected to similar kinase assays. (D) Phosphorylation sites by Erk2. (E) Phosphorylation of Nudel by mitotic cell extracts. Histone H1 served as a control for the quality of the extracts. Kinase assays were performed in the presence or absence of olomoucine, a Cdc2/Erk inhibitor, as indicated.

To distinguish Nudel from NudE, FLAG-tagged Nudel and NudE were expressed in HEK293T cells and were immunoblotted with anti-FLAG M2 antibody. In cells treated with nocodazole to enrich M-phase population, the phosphorylated forms characterized by their slower migration rates were readily detected for both FLAG-Nudel (Fig. 2C, lane1) and FLAG-NudE (lane 5) in addition to unphosphorylated forms due to the existence of interphase cells (Fig. 2C, compare lanes 2 and 6). Both proteins were therefore phosphoproteins in M phase. Furthermore, when the threonine and serine resides in all S/TP motifs of Nudel were mutated into valine or alanine, the phosphorylated form disappeared (Fig. 2B, lane 3). As a control, the percentages of mitotic cells expressing FLAG-Nudel and FLAG-Nudel^{mt5} were comparable after IIF staining of the sample cells. The major phosphorylation sites of Nudel in M phase were therefore located in the S/TP motifs.

Phosphorylation by Cdc2 and Erk2. Cdc2 is a major kinase controlling G_2/M transition (19, 29). Erk forms of MAPK, on the other hand, are important for meiosis progression in addition to their roles in G_0/G_1 transition (1). Although their functions in somatic cell mitosis are less understood, association of activated Erk1 and -2 with kinetochores and asters implies their involvement (37).

Since Nudel and NudE were both phosphorylated in M phase, we first checked if they were substrates of Cdc2 in vitro. As shown in Fig. 3A, incubation of FLAG-tagged NudE (lane 1) and Nudel (lane 2), but not Nudel^{mt5} (lane 3), with purified Cdc2 (New England Biolabs) resulted in incorporation of [^{32}P]phosphate groups. Since three of the five S/TP motifs in Nudel are typical MAPK sites (PXS/TP), we also performed similar assays by using purified Erk2. As shown in Fig. 3B, activated Erk2 (New England Biolabs) also phosphorylated both Nudel (lane 2) and NudE (lane 4) but not Nudel^{mt5} (lane 5). Phosphorylation was not detected in the absence of exogenous kinase (lanes 1 and 3), excluding the possibility of kinase contamination in the immunoprecipitates. The phosphorylation sites of Erk2 therefore also fell into the S/TP motifs.

To further determine the detailed phosphorylation sites, we purified five FLAG-tagged mutants, Nudel^{S1} to Nudel^{S5}. Each mutant contained only one distinct S/TP motif. When these mutants were incubated with purified Cdc2, only Nudel^{S2}, Nudel^{S4}, and Nudel^{S5} were phosphorylated (Fig. 3C). Phosphorylation sites of Erk2 were determined in the same way (Fig. 3D). In this case, only Nudel^{S2} and Nudel^{S5} were phosphorylated. Therefore, T219, S242, and T245 of Nudel were phos-

phorylation sites of Cdc2 in vitro. In contrast, Erk2 only phosphorylated T219 and T245. These two sites, with surrounding sequences such as PATP from residues 217 to 220 and PLTP from 243 to 246, respectively, are indeed typical MAPK sites.

To get further clues for kinases responsible for Nudel phosphorylation in M phase, we performed kinase assays by using mitotic extracts prepared from SMMC-7721 cells (Fig. 3E). As expected, the extracts phosphorylated histone H1 (Fig. 3E, lane 1), and the phosphorylation was completely abolished in the presence of 50 μM olomoucine (lane 2), a potent Cdc2 inhibitor (50% inhibitory concentration, 7 μM), and less-potent Erk1 inhibitor (50% inhibitory concentration, 25 μM) (32). The extracts also phosphorylated FLAG-Nudel (Fig. 3E, lane 4) but not FLAG-Nudel^{mt5} (lane 3). Similarly, phosphorylation of FLAG-Nudel was eliminated in the presence of olomoucine (Fig. 3E, lane 5).

Association with the centrosomes and mitotic spindles. Both Nudel and NudE are centrosome proteins, although noncentrosomal fractions always exist in the cytoplasm (9, 20, 25). Our IgY also consistently recognized centrosomal Nudel and NudE (Fig. 4A, panel 1), which colocalized with the microtubule-organizing center (MTOC) (panel 2).

To further explore their roles in the cell cycle, we expressed GFP-Nudel and GFP-NudE in HEK293 cells so that localization of exogenous proteins could be directly visualized through GFP autofluorescence. High-level expression of either protein resulted in bright punctate distribution in the cytoplasm (data not shown). In contrast, cells expressing moderate to low levels of GFP fusion proteins featured bright juxtanuclear fluorescence dots or speckles (Fig. 4B, panel 1). Some cells had one or two closely spaced dots colocalized with γ-tubulin (Fig. 4B, panels 2 and 3), a centrosome marker (38). The rest showed multiple fluorescence dots clustered together (Fig. 4B, panel 1). In such cells, at least one dot colocalized with γ-tubulin (Fig. 4B, panels 2 and 3), indicating that the dot clusters are located at the centrosome regions. During M phase, the centrosomal association of GFP-Nudel was largely reduced. Instead, a fraction of the protein associated with the mitotic spindle, whereas the rest dispersed in the cytoplasm (Fig. 4B, panels 4 to 6). GFP-NudE behaved in a manner similar to that of GFP-Nudel (Fig. 4B, inlets). Their association with spindles was usually weak but was clearly visible over the background of cytoplasmic fluorescence. As a control, GFP alone failed to target to either the centrosome or the spindle (Fig. 4C, panels 1 to 4).

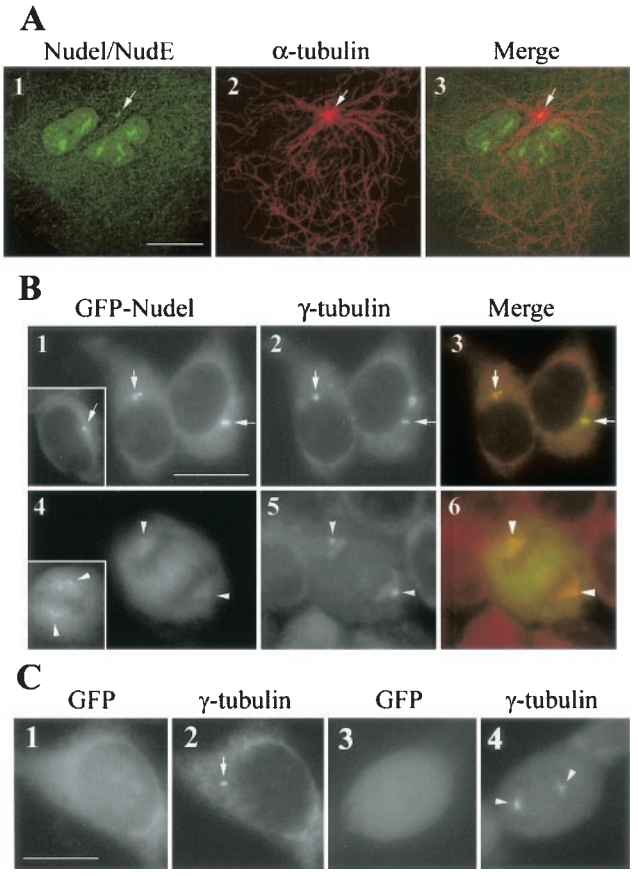

FIG. 4. Association of Nudel and NudE with centrosomes and mitotic spindles. Arrows and arrowheads point to positions of centrosomes and spindle poles, respectively. Scale bar, 10 μm. (A) Confocal images showing the centrosomal staining of anti-Nudel IgY. CV1 cells treated with nocodazole for 30 min were extracted briefly to remove soluble proteins. After fixation, cells were double stained to show Nudel and NudE (panel 1), α-tubulin (panel 2), and the merged image (panel 3). In addition to centrosome localization, some nuclear staining was also visible in panel 1. (B) Subcellular localization of GFP-Nudel and GFP-NudE. HEK293 cells were transiently transfected to express GFP-Nudel (panels 1 and 4) and were labeled with anti-γ-tubulin antibody (panels 2 and 5). Insets show typical GFP-NudE transfectants reduced to 80% of their original sizes. The spindle association of Nudel and NudE was moderately exaggerated for clarity. (C) GFP control. Typical cells in interphase (panels 1 and 2) and M phase (panels 3 and 4) are shown.

Regulation of the subcellular localization by phosphorylation. The coincidence between phosphorylation of Nudel and NudE and the reduced spindle pole localization in M phase implies that phosphorylation may regulate their distribution during the cell cycle. In addition to Nudel^{mt5}, we created another mutant, Nudel^{pmt5}, in which the serine and threonine residues in all S/TP motifs were mutated into glutamic acids to hopefully mimic phosphorylation (7). Effects of phosphorylation on subcellular localization of Nudel were explored by comparing behaviors of the mutants with that of the wild type.

We found that both GFP-Nudel and GFP-Nudel^{mt5} formed bright centrosomal foci in interphase cells (Fig. 5A and B, panels 1 and 2). In contrast, GFP-Nudel^{pmt5} only weakly localized to the centrosomes (Fig. 5C, panels 1 and 2). For quantitative purposes, their centrosomal fluorescence was measured from 10 cells with comparable GFP fluorescence for each protein. Although the values varied from cell to cell, the centrosomal intensities of the first two proteins were generally six- to eightfold higher than those of GFP-Nudel^{pmt5}. From metaphase to anaphase, while a fraction of GFP-Nudel associated with mitotic spindles (Fig. 5A, panels 3 to 6), GFP-Nudel^{mt5} bound preferably to spindle poles (Fig. 5B, panels 3 to 8). GFP-Nudel^{pmt5} behaved like GFP-Nudel during this period (Fig. 5C, panels 3 to 6). In telophase, while the spindle pole localization of GFP-Nudel became apparent (Fig. 5A, panels 7 and 8), GFP-Nudel^{pmt5} still failed to show such localization clearly (Fig. 5C, panels 7 and 8). Phospho-Nudel and Nudel^{pmt5}, which simulated phosphorylation, thus correlated with stronger distribution on spindles at metaphase (Fig. 5,

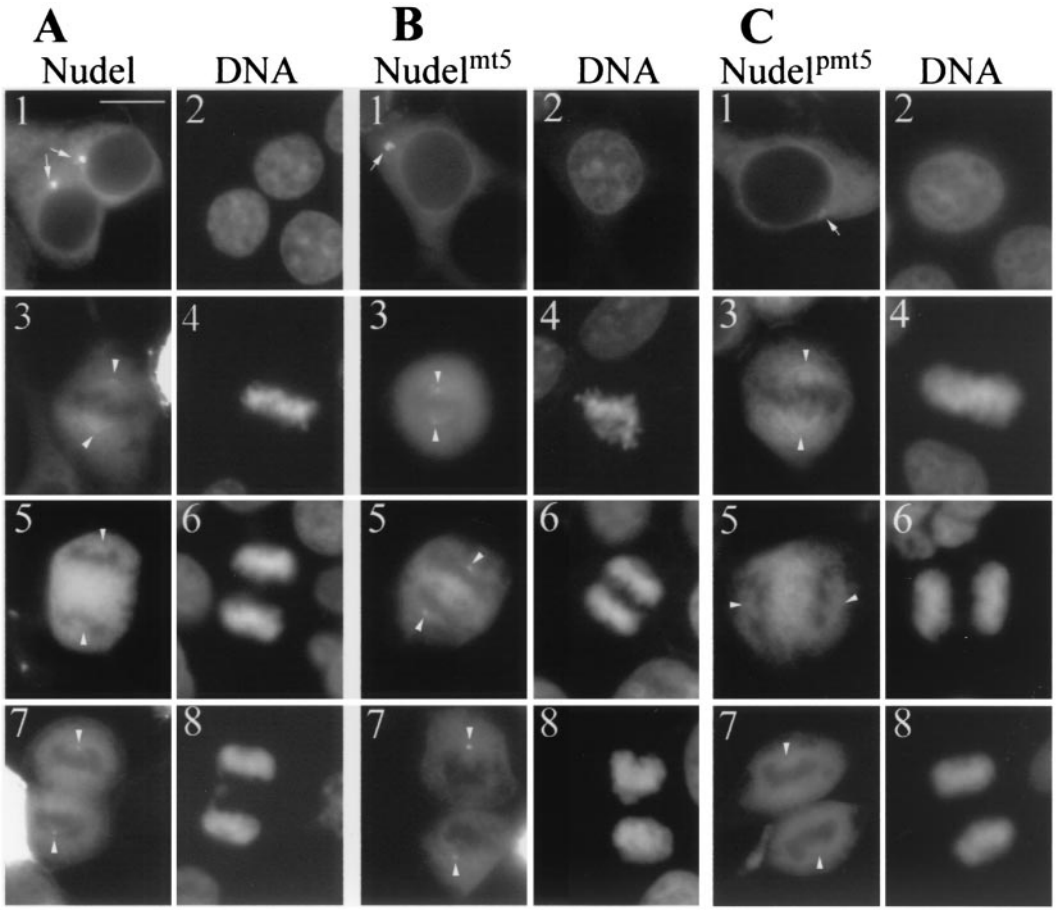

FIG. 5. Phosphorylation regulates localization of Nudel at the centrosomes and mitotic spindles. Typical HEK293T cells expressing GFP-tagged Nudel (A), Nudel^{mt5} (B), or Nudel^{pmt5} (C) are shown for comparison. DNA was stained by DAPI. Panels 1 and 2, interphase cells; panels 3 and 4, metaphase cells; panels 5 and 6, anaphase cells; panels 7 and 8, telophase cells. Arrows and arrowheads indicate positions of centrosomes and spindle poles, respectively, which were marked by IIF of γ-tubulin (data not shown). Scale bar, 10 μm.

panels 3 and 4) and weak association with the MTOC. In contrast, unphosphorylated Nudel in interphase cells and Nudel^{mt5}, which was incapable of phosphorylation, exhibited stronger localization at the MTOC.

To further corroborate these findings, we fractionated centrosomes from HEK293T cells transfected to express each of the three fusion proteins. Immunoblotting indicated that GFP-Nudel was indeed cosedimented with the centrosomal fractions indicated by γ-tubulin (Fig. 6A, lanes 4 to 6), and so were GFP-Nudel^{mt5} and GFP-Nudel^{pmt5} (data not shown). Moreover, although the levels of Nudel and mutants were similar in total cell lysates (Fig. 6B, lanes 1 to 3), GFP-Nudel^{pmt5} exhibited much weaker association with centrosomes (Fig. 6C, lane 3). In contrast, GFP-Nudel and GFP-Nudel^{mt5} exhibited comparable levels in the centrosome fractions (lanes 1 and 2).

Convergence to the spindle poles following depletion of cellular ATP. Nudel and NudE appear as regulatory factors for cytoplasmic dynein through direct interaction (9, 20, 25), although more direct evidence is still required for better understanding of their functional relationship. In mitotic PtK1 cells, the spindle checkpoint proteins, such as Mad2, Bub1, and CENP-E, are constantly transported from kinetochores to spindle poles along spindle microtubules by cytoplasmic dynein

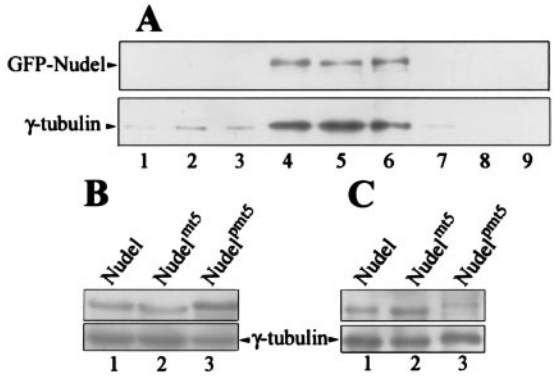

FIG. 6. Association of GFP-Nudel and mutants with centrosome fractions. (A) Copurification of GFP-Nudel with centrosome fractions. Centrosomes were fractionated from HEK293T cells expressing GFP-Nudel as described in Materials and Methods. Fractions with odd numbers from the final sucrose gradient were analyzed for GFP-Nudel (upper panel) and γ-tubulin (lower panel), a centrosome marker, by immunoblotting. (B) Protein levels of GFP-tagged Nudel, Nudel^{mt5}, and Nudel^{pmt5} in cell lysates used for centrosome fractionation. γ-Tubulin (lower panel) in the same blot served as a loading control. (C) Centrosome-associated GFP-Nudel and mutants. The fraction richest in γ-tubulin from each preparation was chosen for comparison.

(13, 14). This dynamic process, which contributes to inactivation of the spindle checkpoint essential for proper anaphase onset, can be visualized by treating cells with azide to reduce cellular ATP to 5 to 10% of normal levels (ATP inhibitor assay). Such a treatment results in depletion of these proteins, including dynein, from kinetochores and subsequent accumulation at spindle poles in a microtubule-dependent manner (13, 14). ATP is important for dissociation of dynein from microtubules (22). Reduction of cellular ATP levels after azide treatment probably impairs this process, leading to accumulation of dynein and its partners or cargos at the extreme minus ends of microtubules or the MTOC. A continuous transport process can therefore be visualized easily. If Nudel and NudE are functional partners of dynein in M phase, they should comigrate with it in the ATP inhibitor assay.

We found that Nudel and NudE were indeed transported to spindle poles after azide treatment in mitotic HEK293T cells. As shown in Fig. 7A, the pattern of GFP was not altered without (panel 1) or with (panel 2) azide treatment. However, GFP-NudE exhibited strong spindle pole localization in azide-treated cells (Fig. 7B, panels 3 to 6) in contrast to mock-treated ones (panels 1 and 2). Star-shaped structures around spindle poles were especially visible in cells at prometaphase (Fig. 7B, panels 3 and 4), suggesting association of GFP-NudE with aster microtubules. GFP-Nudel also showed the similar phenotypes (data not shown). In mock-treated cells, a fraction of dynein exhibited its typical spindle localization (Fig. 7C, panel 2) (14), a pattern resembling that of GFP-Nudel (Fig. 7C, panel 1). Thirty minutes after azide treatment, both proteins were concentrated at the spindle poles (Fig. 7D, panels 1 and 2). Such poleward congression was also observed in cells from anaphase (Fig. 7D, panels 4 to 6) to early telophase (data not shown). At late telophase, however, dynein no longer displayed dramatic accumulation at poles after azide treatment. Instead, the majority of it concentrated in regions around the midbody, where the remains of interdigitated spindle microtubules resided (Fig. 7D, panel 8). A substantial fraction of GFP-Nudel, despite it being in aggregation form, was also distributed in these areas (Fig. 7D, panel 7). Interestingly, GFP-Nudel and GFP-NudE frequently aggregated into numerous foci in both mitotic cells (Fig. 7D and E) and interphase cells (see Fig. 9A) following azide treatment, although the number of foci varied from cell to cell. Such aggregation, however, was not observed in cells expressing GFP alone (Fig. 7A). The above patterns clearly differed from those seen with mock-treated cells (Fig. 7C, panels 4 to 9). These data reinforced the point that Nudel and NudE bound to cytoplasmic dynein and migrated with it to spindle poles.

To further corroborate these results, we treated cells with nocodazole for 3 h to disassemble microtubules prior to ATP inhibitor assay in the presence of nocodazole. As a control, the majority of cellular GFP-Nudel was transported to spindle poles in cells without nocodazole treatment (Fig. 7E). The presence of nocodazole completely blocked the polar transport of Nudel in M phase, indicating that the transport process is indeed microtubule-dependent (Fig. 7F). Aggregation of Nudel following azide treatment, however, was not affected by nocodazole (Fig. 7F).

Involvement in cytoplasmic dynein-mediated poleward transport. To clarify if Nudel and NudE were simply passengers of the dynein motor or active players for dynein function, we created a deletion mutant, GFP-Nudel^{N20}, which lacked amino acids 114 to 133 in the Lis1-binding domain (Fig. 8A) (25). Such deletion completely disrupted Nudel-Lis1 interaction (Fig. 8B) but not Nudel homodimerization (data not shown). Moreover, since the dynein-binding domain between residues 256 to 345 was intact, this mutant should still interact with dynein (25). Time-lapse microscopy showed that, compared to that of wild-type GFP-Nudel (Fig. 7E), accumulation of this mutant at spindle poles after azide treatment was dramatically reduced (Fig. 8C), suggesting impairment of its poleward transport. In either untreated or mock-treated mitotic cells, GFP-Nudel^{N20} did not exhibit clear spindle localization (Fig. 8D, panel 1, and F, panel 1) (data not shown). The typical distribution of dynein on the spindle (Fig. 7C, panel 2) was also disrupted in cells expressing GFP-Nudel^{N20} (Fig. 8D, panel 2). As controls, in the surrounding untransfected mitotic cells of both mock-treated and azide-treated samples, dynein still displayed its typical localization (data not shown). After azide treatment, cytoplasmic dynein also failed to fully congregate at spindle poles (Fig. 8D, panels 4 to 6). Rather, the majority of dynein was trapped on the spindle (Fig. 8D, panel 5), indicating that the poleward movement of dynein was at least partially disrupted by Nudel^{N20}.

We further examined if overexpression of GFP-Nudel^{N20} impaired the poleward transport of spindle checkpoint proteins by dynein. Bub1 is one of the spindle checkpoint proteins transported from kinetochores to spindle poles (14). Due to a lack of appropriate antibodies for IIF, we coexpressed FLAG-Bub1 with GFP-Nudel in HEK293T cells. In intact or mock-treated metaphase cells, a portion of FLAG-Bub1 showed distribution on the spindle similar to that of GFP-Nudel (Fig. 8E, panel 1 to 3 and data not shown). Its kinetochore localization was hardly visible at this stage. After azide treatment both Bub1 and Nudel displayed strong accumulation at spindle poles as discrete speckles (Fig. 8E, panels 4 to 6). However, coexpression with GFP-Nudel^{N20} led to inhibition of the poleward transport of FLAG-Bub1 (Fig. 8F, panels 4 to 6). Although some proteins were accumulated at spindle poles, a substantial amount of FLAG-Bub1 was distributed on the entire spindle (Fig. 8F, panel 5), resembling the pattern of dynein (Fig. 8D, panel 5). In addition, the spindle localization of FLAG-Bub1 was also disrupted in control cells (Fig. 8F, panel 2). These data indicated a clear role of Nudel for the activities of the dynein motor during M phase.

Effects of Nudel phosphorylation on its dynein-mediated transport and Lis1-binding activity. To further explore how phosphorylation affected Nudel functions, we first examined if phosphorylation affected accumulation of Nudel at the MTOC. Time-lapse microscopy revealed dramatic intensification of centrosomal fluorescence of GFP-tagged Nudel, Nudel^{mt5}, and Nudel^{pmt5} following the time of azide treatment in both mitotic cells (data not shown) and interphase cells (Fig. 9A), indicating that the phosphorylation status of Nudel is not critical for dynein function. In mitotic cells, their average accumulation rates were sequentially 3,495 ± 536/min (means ± standard deviations) (n = 4), 1,553 ± 354/min (n = 5), and 1,935 ± 403/min (n = 8) according to our studies with time-lapse microscopy. For the interphase cells shown in Fig. 9A, the quan-

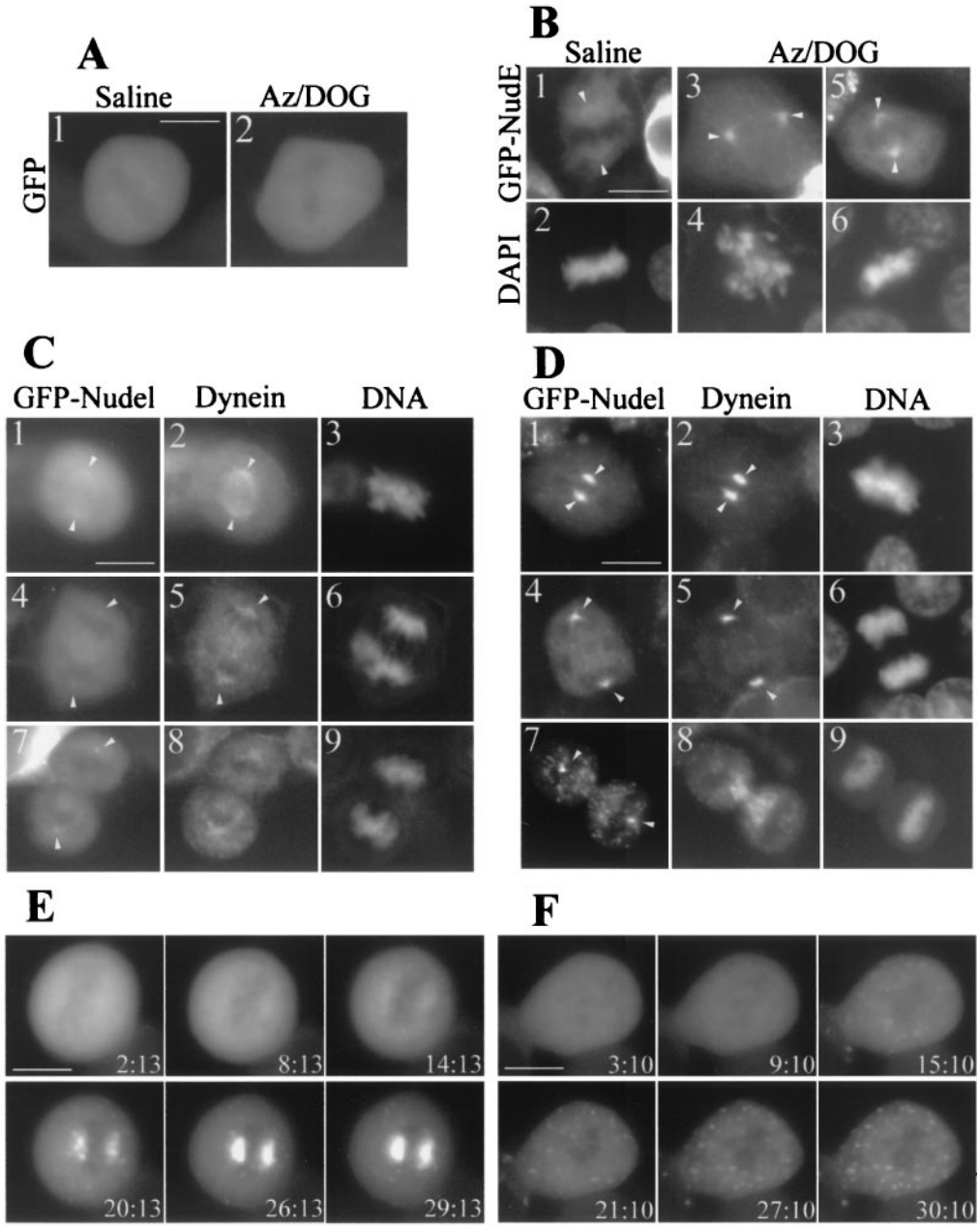

FIG. 7. Transport of Nudel and NudE to spindle poles along microtubules. HEK293T cells transfected with appropriate plasmids for 36 h were treated with phosphate-buffered saline (saline) or phosphate-buffered saline containing Na-azide and DOG (Az/DOG) for 30 min at 37°C. Cells were either fixed by methanol (B, C, and D) or recorded live (A, E, and F) after the indicated treatment. DNA was stained by DAPI. Arrowheads point to spindle poles. Scale bar, 10 μm. (A) Mitotic cells expressing GFP. (B) Mitotic cells expressing GFP-NudE. A typical cell in prometaphase (panels 3 and 4) or metaphase (panels 5 and 6) after azide treatment is shown. (C) Mitotic cells expressing GFP-Nudel and treated with saline to serve as controls for panel D. Cytoplasmic dynein was decorated with anti-DIC antibody. (D) Mitotic cells expressing GFP-Nudel after ATP inhibitor assay. (E) Time-lapse images of a mitotic cell mock treated with DMSO to serve as controls for panel F. Images were recorded live every 3 min following Az/DOG treatment. (F) Microtubule-dependent accumulation of Nudel at spindle poles. Cells expressing GFP-Nudel were treated with Az/DOG and nocodazole after preincubation with nocodazole for 3 h to disassemble microtubules.

titative data for their centrosomal fluorescence intensities are listed in Fig. 9B. According to these results, we propose that phosphorylated Nudel exhibits a higher dissociation rate from the MTOC and therefore weaker localization at spindle poles (see Discussion).

For clues at the molecular level, we performed coimmunoprecipitation to check interactions between Nudel, Lis1, and dynein. As shown in Fig. 9C, FLAG-Nudel^{pmt5} reproducibly pulled down much more endogenous Lis1 than FLAG-tagged mt5 mutant or wild-type Nudel did in interphase (lanes 2 to 4), although their protein levels were constant in the total cell lysates (data not shown). To further corroborate these results,

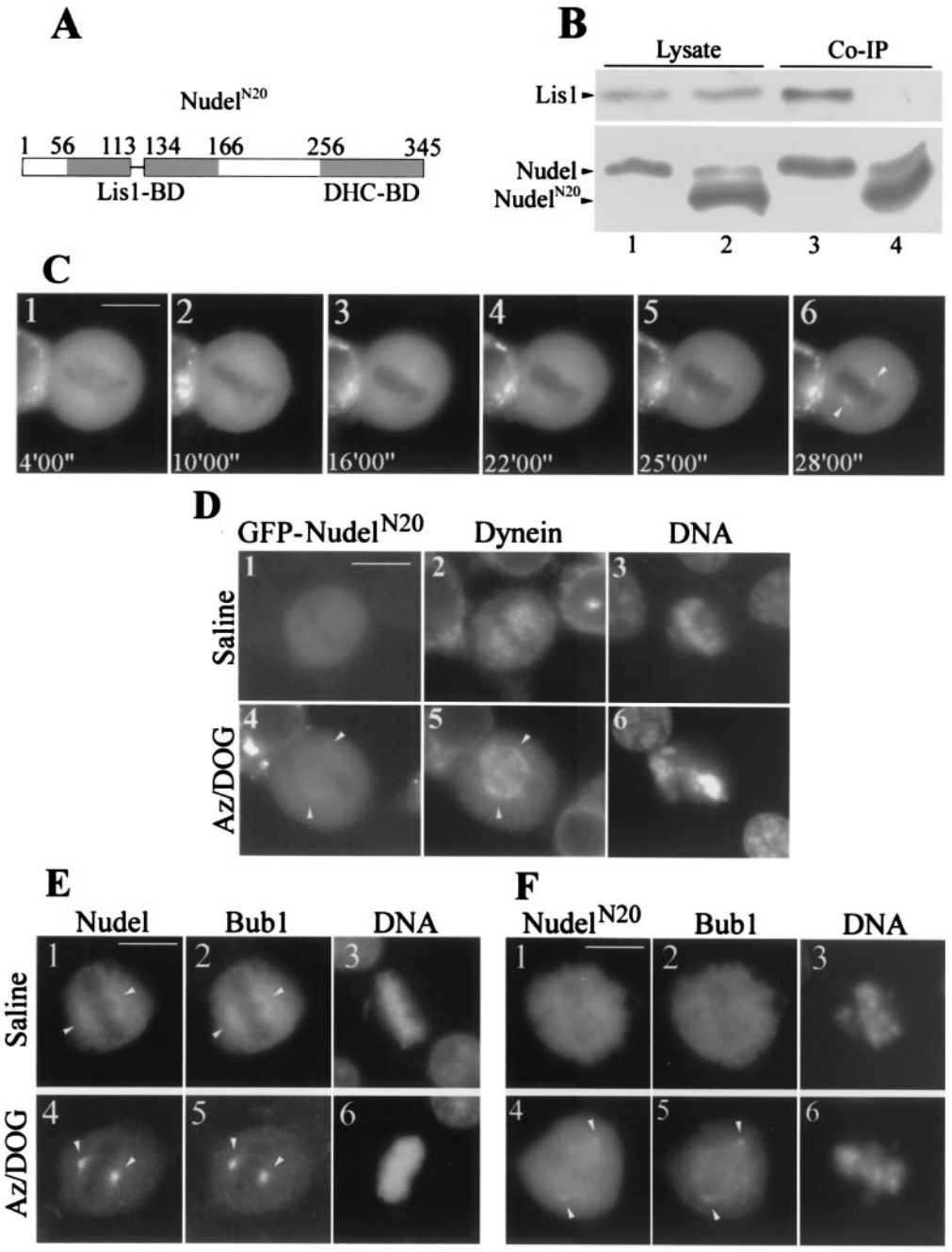

FIG. 8. Involvement of Nudel in dynein-mediated poleward transport. Arrowheads point to spindle poles. Scale bar, 10 μm. (A) Diagram of Nudel^{N20}. BD, binding domain. (B) Loss of interaction between Nudel^{N20} and Lis1. HEK293T cells coexpressing HA-Lis1 with either FLAG-Nudel (lane 1) or FLAG-Nudel^{N20} (lane 2) were subjected to coimmunoprecipitation (Co-IP, lanes 3 and 4) with anti-FLAG beads. The slow migration bands in lanes 2 and 4 are probably a phosphorylated form that was readily detected when samples were overloaded. (C) A typical mitotic HEK293T cell expressing GFP-Nudel^{N20} following Az/DOG treatment. (D) Abnormal spindle distribution and poleward movement of cytoplasmic dynein in GFP-Nudel^{N20} transfectants. (E) Distribution and poleward transport of FLAG-Bub1 in GFP-Nudel transfectants. (F) Impaired distribution and transport of FLAG-Bub1 in cells coexpressing GFP-Nudel^{N20}.

transfected cells were treated with nocodazole to enrich M-phase population. Microscopic examination indicated that about 50% of transfectants on average were arrested in prometaphase after 12 h of treatment. Since poor attachment of HEK293T cells to culture dishes precluded shake off of the mitotic cells, whole populations were assayed. In this case, both the pmt5 mutant and Nudel brought down more Lis1 than the mt5 mutant did (Fig. 9C, lanes 5 to 7). DIC was detected in the immunocomplexes as faint bands only after extensive incubation (overnight) during immunoprecipitation (Fig. 9). These data indicate that phospho-Nudel binds to Lis1 more efficiently. This conclusion is also consistent with the slightly stronger association of Lis1 with FLAG-Nudel than with the mt5 mutant (Fig. 9C, lanes 3 and 4), because a small fraction

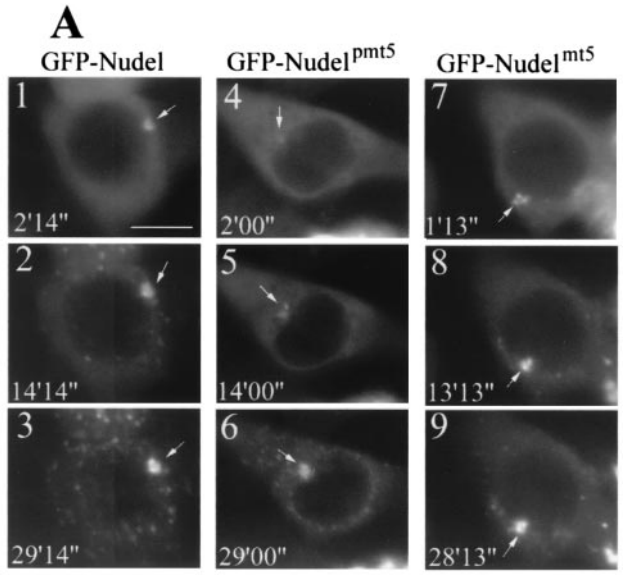

B

	Nudel	Nudel^{pmt5}	Nudel^{mt5}
Initial intensities	10348	896	11291
Final intensities	38684	18903	31460
Increase (folds)	3.7	21.1	2.8
Accumulation rates	1050/min	667/min	747/min

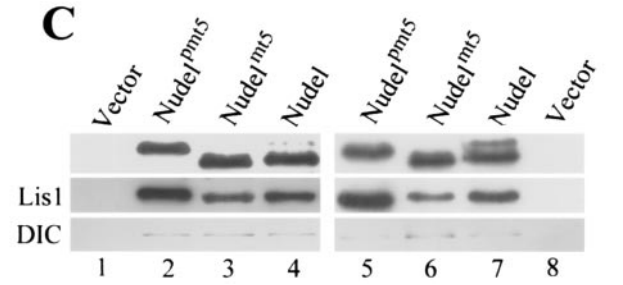

FIG. 9. Effects of Nudel phosphorylation on azide-induced convergence to centrosomes and Lis1-binding activity. (A) Time-lapse images for interphase cells expressing the indicated proteins. Images were recorded live every 3 min following ATP inhibitor assays. Positions of the centrosome are indicated by arrows. Scale bar, 10 μm. (B) Quantitative data for the cells shown in panel A. The centrosomal fluorescence intensities were presented as gross brightness after subtraction of backgrounds. Average accumulation rates = (final intensities − initial intensities)/time duration. (C) Coimmunoprecipitation with FLAG-tagged Nudel and mutants. Approximately 2×10^7 HEK293T cells transfected to express each of the indicated forms of Nudel were either lysed directly (lanes 2 and 4) or treated with nocodazole for 12 h before lysis (lanes 5 and 7). Cells transfected with vector served as controls (lanes 1 and 8). The lysates were subjected to immunoprecipitation with anti-FLAG beads. Immunoblotting was then performed with anti-FLAG (upper panel), anti-Lis1 (middle panel), or anti-DIC (lower panel) antibodies. Phospho-Nudel showed slower migration rate in lanes 4 and 7 (upper panel).

of Nudel was phosphorylated (lane 4, upper panel) due to the existence of mitotic cells in the population.

DISCUSSION

Phosphorylation of Nudel and NudE in M phase. Nudel and NudE appear to be mainly phosphorylated at S/TP motifs by proline-dependent serine/threonine kinases. In neurons, Nudel is the only known in vivo substrate of Cdk5/p35 (20, 25), a key kinase for neuronal migration (3, 4, 27). Nudel colocalizes with Cdk5 in axonal growth cones and cell bodies of cultured embryonic hippocampal neurons. Phosphorylation by Cdk5 alters localization patterns of Nudel in neurites (20). In vitro study suggests that the phosphorylation sites are Ser-198, Thr-219, and Ser-231, located in the first three S/TP motifs (20). Phosphorylation regulation of Nudel may link the Cdk5/p35 pathway of neuronal migration to the Lis1/cytoplasmic dynein pathway during development of the CNS (20, 25).

We found that Nudel and NudE were also phosphorylated in M phase (Fig. 2 and 3). First, Nudel and NudE were specifically phosphorylated in M phase. Moreover, both proteins were phosphorylated by Cdc2 and Erk2 in vitro. In the case of Nudel, the phosphorylation sites were also located in the S/TP motifs. Detailed mutagenesis study indicated that T219, S242, and T245 were phosphorylated by Cdc2, while T219 and T245 were phosphorylated by Erk2. Among these three sites, only T219 is also phosphorylated by Cdk5 (20). Such differences imply distinct influences on Nudel functions by these kinases. Moreover, the results from assays that used mitotic cell extracts strongly suggest the in vivo phosphorylation sites also in the S/TP motifs of Nudel. Inhibition of the phosphorylation by Cdc2 and Erk1 and -2 inhibitor olomoucine is consistent with results of our in vitro kinase assays, suggesting that Cdc2 and probably also Erk1 and -2 may be the major kinase(s) for Nudel in M phase. Due to conservation of the S/TP motifs, NudE may also be phosphorylated at similar sites by these kinases, though it contains an additional potential Cdk site at S282 (SPNR).

Biological effects of phosphorylation. We demonstrated that Nudel and NudE are subjected to cell-cycle-dependent redistribution in HEK293T cells. In interphase, both proteins strongly associated with centrosomes (Fig. 4 and 5) (9, 20, 25). In contrast, their association with spindle poles was weak in M phase, while association with the spindle was observed from prometaphase to early anaphase (Fig. 4 and 5). Although Nudel interacts with γ-tubulin (data not shown) (9), both proteins did not always colocalize with each other at centrosomes when Nudel was overexpressed (Fig. 4). Formation of γ-tubulin-independent centrosomal foci of GFP-Nudel suggests the existence of another protein partner(s), such as Lis1, at centrosome regions (20, 25). Alternatively, these foci might be Nudel aggregates due to overexpression. Nevertheless, in contrast to results of a previous report (9), overexpression of Nudel or NudE did not significantly affect the centrosomal localization of γ-tubulin in CV1 and HEK293 cells (Fig. 4 and data not shown).

Phosphorylation influenced the cellular dynamics of Nudel during the cell cycle. To our satisfaction, the mt5 and pmt5 mutants indeed behaved like unphosphorylated and phosphorylated forms, respectively, of Nudel in cells. The stronger localization of Nudel^{mt5} and unphosphorylated Nudel at the MTOC in contrast to Nudel^{pmt5} and phospho-Nudel suggests that the phosphorylation alone is sufficient to significantly reduce the centrosomal association of Nudel in both interphase and M-phase cells (Fig. 5 and 6). Since the fluorescence intensities at the MTOC actually reflect the steady-state levels or the net effects of dynamic association-dissociation processes of

Nudel, stronger localization stands for a lower dissociation rate at the MTOC. During ATP inhibitor assays, GFP-tagged Nudel and the two mutants accumulated dramatically at the MTOC, especially in mitotic cells (Fig. 7E and data not shown), in which the initial intensities at spindle poles were very low. Their dissociation rates are therefore negligible during the assays. In another words, under the circumstances, their accumulation rates should somewhat reflect those of intact mitotic cells. In fact, such values were comparable between the two mutants (1,553 ± 354/min for the mt5 mutant and 1,935 ± 403/min for the pmt5 mutant). The values were also similar for the two interphase cells in Fig. 9A (also see Fig. 9B). If their dissociation rates were also comparable, both proteins would have exhibited similar steady-state levels at centrosomes. The levels, however, actually differed 12.6-fold (Fig. 9A and B). It is therefore reasonable to propose that phosphorylation strongly augments the dissociation rate of Nudel at the MTOC but has little effect on its accumulation rate. Moreover, the accumulation rates of the mutants were approximately twofold lower than those of GFP-Nudel in both mitotic and interphase cells. This variation may be attributed to the disturbance of mutagenesis on Nudel conformation and properties. Even in the case of Nudel, its 11.5-fold difference from Nudel^{pmt5} at centrosomes (Fig. 9A and B) still favors our explanation. Whether Nudel phosphorylation also regulates the dynamics of dynein at the MTOC, however, still remains to be shown.

Phosphorylation of Nudel in M phase appears to positively modulate dynein motor activity. Both phosphorylated and unphosphorylated forms of Nudel were transported by dynein (Fig. 7 and 9 and data not shown), indicating that neither of them inactivated the dynein motor. On the other hand, both phospho-Nudel and Nudel^{pmt5} bound Lis1 more strongly than Nudel or Nudel^{mt5} did (Fig. 9C). Since Lis1 binds to DIC and two independent sites in DHC (25, 31), multiple Lis1 molecules may exist in a dynein complex. Multiple Nudel molecules may also exist in dynein through homodimerization, interaction with the P1-loop or the C-terminal portion of DHC, or interaction with Lis1 (20, 25). One piece of preliminary evidence for this is the movement of Nudel aggregates toward the MTOC (Fig. 7E and 9A and data not shown) and other dynein-rich regions (Fig. 7D, panels 7 and 8), while dynein did not show similar discrete staining (Fig. 7D, panels 7 and 8, and data not shown). The phospho-Nudel in M phase may therefore function to facilitate Lis1 binding to the dynein complex, subsequently leading to a mutual increase of their stoichiometry. Changes of Lis1 stoichiometry may then modulate dynein activity, as implicated by studies on Lis1-deficient mice and Lis1 overexpression (8, 12, 28). The importance of Nudel-Lis1 interaction for the poleward movement of dynein (Fig. 8) further supports this speculation. Why such modulation for dynein activity is to occur in M phase, however, remains to be elucidated. It also remains to be seen if phosphorylation of Nudel in neurons by Cdk5/p35 (20, 25) has similar effects on the Lis1-binding activity.

We also noticed that, with short incubation time in our immunoprecipitation experiments, dynein was not detected in the immunocomplex in spite of its relative abundance in the lysates (data not shown). Lis1, however, was readily visible as strong bands. Substantial amounts of Nudel and Lis1 therefore appear to exist as heterodimers free of dynein in cells.

Involvement in dynein-mediated transport in M phase. Cytoplasmic dynein plays multiple roles in M phase. Dynein is essential for spindle assembly and orientation (16, 17). It may also function in chromosome segregation during anaphase (16). Recently, it has been shown to mediate transport of kinetochore checkpoint proteins, including Bub1 and Mad2, to spindle poles along microtubules, a process that contributes to inactivation of the spindle checkpoint (13, 14).

Our results indicate that Nudel and NudE are functional partners of cytoplasmic dynein during the poleward transport process. First, Nudel and NudE were also transported to spindle poles as revealed by ATP inhibitor assay (Fig. 7). Association of some Nudel and NudE with aster-like structures and the requirement of the intact microtubule arrays for transport strongly suggest their binding to and migrating along spindle microtubules. Their bipolar accumulation in cells from prometaphase to telophase indicates that the transport actually persists throughout these stages (Fig. 7D). The coincidence between reduction of the cytoplasmic fluorescence and increase of the spindle pole fluorescence during ATP inhibitor assays also suggests transport of the cytoplasmic pools of Nudel to spindle poles (Fig. 7E). Second, GFP-Nudel and GFP-NudE colocalized with cytoplasmic dynein on spindles (Fig. 7C; data not shown). After azide treatment, they again colocalized at spindle poles. As binding partners of dynein, such colocalization strongly suggests direct interactions with dynein during the transport process. In addition, the azide-dependent accumulation of dynein at poles was also observed in anaphase (Fig. 7D). In late telophase, although dynein was less striking at the poles, it did migrate to the regions containing remnants of the antiparallel spindle microtubules (Fig. 7D). These results strongly suggest that the dynein-mediated transport along spindles is a constitutive process throughout M phase.

Finally, impairment of the poleward transport by the mutant Nudel^{N20} further indicates that Nudel is involved in the motor function of dynein (Fig. 8). GTP-Nudel^{N20}, which lacked only 20 residues, was no longer transported efficiently to spindle poles in ATP inhibitor assays (Fig. 8). Moreover, the typical spindle localization of cytoplasmic dynein was abolished in cells expressing this mutant. Dynein also lost its ability to fully concentrate at spindle poles in ATP inhibitor assays. Instead, it was accumulated on entire spindles, including poles. Such a phenotype strongly suggests that the motor activity, but not the microtubule-binding ability, is impaired. The trace amount of dynein and GTP-Nudel^{N20} at spindle poles may be due to the existence of endogenous Nudel and NudE and/or residual motor activities of dynein. Nudel^{N20} selectively interacted with dynein but not Lis1 (Fig. 8A and B) (25). Moreover, its homodimerization activity was not abolished (data not shown). Nudel-Lis1 interaction therefore is critical to the dynein motor activity, though Lis1 binds to dynein by itself (25, 31). In fact, Lis1 also exhibited similar poleward transport after azide treatment (data not shown). Nudel and Lis1 therefore serve as regulators of the dynein motor in mitosis. Moreover, comparative studies suggest that NudE may have similar functions in M phase.

As expected, expression of Nudel^{N20} also disrupted distribution of FLAG-Bub1 on spindles and attenuated the poleward transport of the kinetochore checkpoint protein Bub1 (Fig. 8E and F). Again, existence of some Bub1 at spindle

poles after azide treatment may be due to endogenous Nudel and NudE and/or residual motor activities of dynein. It is likely that other spindle checkpoint proteins to be transported by dynein are also affected. It will thus be interesting to further study if and how mitotic progressions are affected in these cells.

It is interesting that Nudel and NudE actually did not exhibit detectable kinetochore localization (Fig. 4 and 5). In contrast, cytoplasmic dynein and Lis1 transiently associate with kinetochores in early M phase (8, 14, 31). Since Lis1-Nudel interaction is important for dynein motor activity, kinetochore proteins should not be transported efficiently without Nudel or NudE on kinetochores. A plausible hypothesis is that Nudel and NudE only transiently bind to kinetochores to trigger or boost the poleward movement through interactions with kinetochore forms of Lis1 and dynein. Certainly, more solid evidence is required to clarify this issue.

ACKNOWLEDGMENTS

We thank Min Qian for technical assistance, Weiqi Xu for help in fluorescence microscopy, and Yongli Shan and Yan Li for proofreading the manuscript. We also thank X. Yao at University of Science and Technology of China for Bub1 cDNA.

This work was supported by grants 30025021 and 39970160 from the National Science Foundation of China, grant KSCX2-2-02 from the Chinese Academy of Sciences, and cross-disciplinary National Basic Research Priorities Program from the Ministry of Science and Technology.

REFERENCES

1. **Abrieu, A., M. Doree, and D. Fisher.** 2001. The interplay between cyclin-B-Cdc2 kinase (MPF) and MAP kinase during maturation of oocytes. J. Cell Sci. **114:**257–267.
2. **Beckwith, S. M., C. H. Roghi, B. Liu, and N. R. Morris.** 1998. The "8-kD" cytoplasmic dynein light chain is required for nuclear migration and for dynein heavy chain localization in Aspergillus nidulans. J. Cell Biol. **143:** 1239–1247.
3. **Chae, T., Y. T. Kwon, R. Bronson, P. Dikkes, E. Li, and L.-H. Tsai.** 1997. Mice lacking p35, a neuronal specific activator of Cdk5, display cortical lamination defects, seizures, and adult lethality. Neuron **18:**29–42.
4. **Dhavan, R., and L.-H. Tsai.** 2001. A decade of CDK5. Nat. Rev. Mol. Cell Biol. **2:**749–759.
5. **Dujardin, D. L., and R. B. Vallee.** 2002. Dynein at the cortex. Curr. Opin. Cell Biol. **14:**44–49.
6. **Efimov, V. P., and N. R. Morris.** 2000. The Lis1-related NUDF protein of *Aspergillus nidulans* interacts with the coiled-coil domain of the NUDE/RO11 protein. J. Cell Biol. **3:**681–688.
7. **Eidenmuller, J., T. Fath, T. Maas, M. Pool, E. Sontag, and R. Brandt.** 2001. Phosphorylation-mimicking glutamate clusters in the proline-rich region are sufficient to simulate the functional deficiencies of hyperphosphorylated tau protein. Biochem. J. **357:**759–767.
8. **Faulkner, N. E., D. L. Dujardin, C. Tai, K. T. Vaughan, C. B. O'Connell, Y. Wang, and R. B. Vallee.** 2000. A role for the lissencephaly gene LIS1 in mitosis and cytoplasmic dynein function. Nat. Cell Biol. **2:**784–791.
9. **Feng, Y., E. C. Olson, P. T. Stukenberg, L. A. Flanagan, M. W. Kirschner, and C. A. Walsh.** 2000. LIS1 regulates CNS lamination by interacting with mNudE, a central component of the centrosome. Neuron **28:**665–679.
10. **Gassmann, M., P. Thommes, T. Weiser, and U. Hubscher.** 1990. Efficient production of chicken egg yolk antibodies against a conserved mammalian protein. FASEB J. **4:**2528–2532.
11. **Hirokawa, N.** 1998. Kinesin and dynein superfamily proteins and the mechanism of organelle transport. Science **279:**519–526.
12. **Hirotsune, S., M. W. Fleck, M. J. Gambello, G. J. Bix, A. Chen, G. D. Clark, D. H. Ledbetter, C. J. McBain, and A. Wynshaw-Boris.** 1998. Graded reduction of Pafah1b1 (Lis1) activity results in neuronal migration defects and early embryonic lethality. Nat. Genet. **19:**333–339.
13. **Howell, B. J., D. B. Hoffman, G. Fang, A. W. Murray, and E. D. Salmon.** 2000. Visualization of Mad2 dynamics at kinetochores, along spindle fibers, and at spindle poles in living cells. J. Cell Biol. **150:**1233–1249.
14. **Howell, B. J., B. F. McEwen, J. C. Canman, D. B. Hoffman, E. M. Farrar, C. L. Rieder, and E. D. Salmon.** 2001. Cytoplasmic dynein/dynactin drives kinetochore protein transport to the spindle poles and has a role in mitotic spindle checkpoint inactivation. J. Cell Biol. **155:**1159–1172.
15. **Inouse, S., B. G. Turgeon, O. C. Yoder, and J. R. Aist.** 1998. Role of fungal dynein in hyphal growth, microtubule organization, spindle pole body motility and nuclear migration. J. Cell Sci. **111:**1555–1566.
16. **Karki, S., and E. L. Holzbaur.** 1999. Cytoplasmic dynein and dynactin in cell division and intracellular transport. Curr. Opin. Cell Biol. **11:**45–53.
17. **Merdes, A., and D. W. Cleveland.** 1997. Pathways of spindle pole formation: different mechanisms; conserved components. J. Cell Biol. **138:**953–956.
18. **Moudjou, M., and M. Bornens.** 1998. Method of centrosome isolation from cultured animal cells, p. 111–119. *In* J. E. Celis (ed.), Cell biology: a laboratory handbook, vol. 2. Academic Press, London, United Kingdom.
19. **Nasmyth, K.** 1996. Viewpoint: putting the cell cycle in order. Science **274:** 1643–1645.
20. **Niethammer, M., D. S. Smith, R. Ayala, J. Peng, J. Ko, M.-S. Lee, M. Morabito, and L.-H. Tsai.** 2000. Nudel is a novel Cdk5 substrate that associates with LIS1 and cytoplasmic dynein. Neuron **28:**697–711.
21. **Pagano, M., R. Pepperkok, J. Lukas, V. Baldin, W. Ansorge, J. Bartek, and G. Draetla.** 1993. Regulation of the cell cycle by the cdk2 protein kinase in cultured human fibroblasts. J. Cell Biol. **121:**101–111.
22. **Porter, M. E., and K. A. Johnson.** 1983. Transient state kinetic analysis of the ATP-induced dissociation of the dynein-microtubule complex. J. Biol. Chem. **258:**6582–6587.
23. **Reiner, O., R. Carrozzo, Y. Shen, M. Wehnert, F. Faustinella, W. B. Dobyns, C. T. Caskey, and D. H. Ledbetter.** 1993. Isolation of a Miller-Dieker lissencephaly gene containing G protein beta-subunit-like repeats. Nature **364:** 717–721.
24. **Reiner, O., and T. Sapir.** 1998. Abnormal cortical development: towards elucidation of the lis1 gene product function. Int. J. Mol. Med. **1:**849–853.
25. **Sasaki, S., A. Shionoya, M. Ishida, M. J. Gambello, J. Yingling, A. Wynshaw-Boris, and S. Hirotsune.** 2000. A LIS1/NUDEL/cytoplasmic dynein heavy chain complex in the developing and adult nervous system. Neuron **28:**681–696.
26. **Smith, D. E., and P. T. Fisher.** 1984. Identification, developmental regulation, and response to heat shock of two antigenically related forms of a major nuclear envelope protein in Drosophila embryos: application of an improved method for affinity purification of antibodies using polypeptides immobilized on nitrocellulose blots. J. Cell Biol. **99:**20–28.
27. **Smith, D. S., P. L. Greer, and L.-H. Tsai.** 2001. Cdk5 on the brain. Cell Growth Differ. **12:**277–283.
28. **Smith, D. S., M. Niethammer, R. Ayala, Y. Zhou, M. J. Gambello, A. Wynshaw-Boris, and L.-H. Tsai.** 2000. Regulation of cytoplasmic dynein behavior and microtubule organization by mammalian Lis1. Nat. Cell Biol. **2:**767–775.
29. **Smits, V. A., and R. H. Medema.** 2001. Checking out the G(2)/M transition. Biochim. Biophys. Acta **1519:**1–12.
30. **Stukenberg, P. T., K. D. Lustig, T. J. McGarry, R. W. King, J. Kuang, and M. W. Kirschner.** 1997. Systematic identification of mitotic phosphoproteins. Curr. Biol. **7:**338–348.
31. **Tai, C.- Y., D. L. Dujardin, N. E. Faulkner, and R. B. Vallee.** 2002. Role of dynein, dynactin, and CLIP-170 interactions in Lis1 kinetochore function. J. Cell Biol. **156:**959–968.
32. **Vesely, J., L. Havlicek, M. Strnad, J. J. Blow, A. Donella-Deana, L. Pinna, D. S. Letham, J. Kato, L. Detivaud, S. Leclerc, et al.** 1994. Inhibition of cyclin-dependent kinases by purine analogues. Eur. J. Biochem. **224:**771–786.
33. **Willins, D. A., B. Liu, X. Xiang, and N. R. Morris.** 1997. Mutations in the heavy chain of cytoplasmic dynein suppress the nudF nuclear migration mutation of Aspergillus nidulans. Mol. Gen. Genet. **255:**194–200.
34. **Xiang, X., S. M. Beckwith, and N. R. Morris.** 1994. Cytoplasmic dynein is involved in nuclear migration in Aspergillus nidulans. Proc. Natl. Acad. Sci. USA **91:**2100–2104.
35. **Xiang, X., W. Zuo, V. P. Efimov, and N. R. Morris.** 1999. Isolation of a new set of Aspergillus nidulans mutants defective in nuclear migration. Curr. Genet. **35:**26–30.
36. **Young, A., J. B. Dictenberg, A. Purohit, R. Tuf, and S. J. Doxsey.** 2000. Cytoplasmic dynein-mediated assembly of pericentrin and gamma tubulin onto centrosomes. Mol. Biol. Cell **11:**2047–2056.
37. **Zecevic, M., A. D. Catling, S. T. Eblen, L. Renzi, J. C. Hittle, T. J. Yen, G. J. Gorbsky, and M. J. Weber.** 1998. Active MAP kinase in mitosis: localization at kinetochores and association with the motor protein CENP-E. J. Cell Biol. **142:**1547–1558.
38. **Zheng, Y., M. L. Wong, B. Alberts, and T. Mitchison.** 1995. Nucleation of microtubule assembly by a γ-tubulin-containing ring complex. Nature **378:** 578–583.
39. **Zhou, Q., D. Chen, E. Pierstorff, and K. Luo.** 1998. Transcription elongation factor P-TEFb mediates Tat activation of HIV-1 transcription at multiple stages. EMBO J. **17:**3681–3691.
40. **Zhu, X., M. A. Mancini, K.-H. Chang, C. Y. Liu, C. F. Chen, B. Shan, D. Jones, T. L. Yang-Feng, and W.-H. Lee.** 1995. Characterization of a novel 350Kda nuclear phosphoprotein that is specifically involved in mitotic-phase progression. Mol. Cell. Biol. **15:**5017–5029.
41. **Zhu, X., L. Ding, and G. Pei.** 1997. Carboxyl terminus of mitosin is sufficient to confer spindle pole localization. J. Cell. Biochem. **66:**441–449.
42. **Zhu, X.** 1999. Structural requirements and dynamics of mitosin-kinetochore interaction in M phase. Mol. Cell. Biol. **19:**1016–1024.